Journal of Mechanical Science and Technology 34 (6) 2020

Original Article
DOI 10.1007/s12206-020-0523-7

Keywords:
· Internal gear pair
· Mesh stiffness
· Finite element method
· Analytical contact theory

Correspondence to:
Lehao Chang
changlehao@chd.edu.cn

Citation:
Feng, S., Chang, L., He, Z. (2020). A hybrid finite element and analytical model for determining the mesh stiffness of internal gear pairs. Journal of Mechanical Science and Technology 34 (6) (2020) 2477~2485.
http://doi.org/10.1007/s12206-020-0523-7

Received August 4th, 2019
Revised February 14th, 2020
Accepted March 28th, 2020

† Recommended by Editor Seungjae Min

A hybrid finite element and analytical model for determining the mesh stiffness of internal gear pairs

Shuo Feng[1], Lehao Chang[1,2] and Zhaoxia He[1]

[1]Key Laboratory of Road Construction Technology and Equipment of Ministry of Education, Chang'an University, Xi'an 710064, China, [2]Shaanxi Hande Axle Company Limited, Xi'an 710201, China

Abstract This work developed an efficient model for calculating the mesh stiffness of spur/helical internal gear pairs by combining the finite element method (FEM) and analytical formula. The tooth global deformation is obtained by separation of the deformation of a full finite element model and a partial model, and the local contact deformation is derived by an analytical line contact formula based on Hertz contact theory. The transmission error and mesh stiffness of the gear pair can be acquired after solving the nonlinear contact equilibrium equations. Compared with the conventional FEM, the proposed method has much smaller computational consumption. Furthermore, it also overcomes the disadvantage that the analytical method is difficult to consider different ring gear structures. Then the influences of ring thicknesses and the number of support pins of the ring gear on the mesh stiffness are discussed. The results show that the ring flexibility will change the amplitude-frequency components of the mesh stiffness a lot.

1. Introduction

Planetary gear trains (PGT) are used in many industrial applications because of their compact structures, low vibration and noise, large power density and high transmission efficiency, especially in high-speed and heavy-duty situations. As an important part of PGT, accurate prediction of the mesh stiffness for external and internal gear pairs is essential for the strength checking and low vibration design. According to the frequently used formula recommended in ISO 6336, only the stiffness of a single tooth pair and the average mesh stiffness can be obtained. To predict the system vibration more accurately, the time varying mesh stiffness needs to be obtained both for external and internal gear pairs.

The previous studies on gear mesh stiffness mainly focused on external gear pairs. The classical analytical methods (AM) in early studies included the widely used formulae proposed by Weber [1] and Ishikawa [2]. Terauchi [3] proposed a method to calculate the tooth deflection and stiffness of spur gears based on conformal mapping functions of tooth profile. Sainsot [4] proposed a supplementary analytical formula for Weber's method to get more accurate gear body-induced tooth deflections. However, these models can be used only for spur gears. Börner [5], Wan [6], Wang [7] and Feng [8] used the thin slice theory to calculate the mesh stiffness of helical gears, and the deflection of each thin slice was obtained by the formulae used for spur gears. The main problem of these models is that they cannot take into account the complex gear body structures, such as special shaped rims, webs and lightening holes. On the other hand, finite element method (FEM) [9-11] can solve this problem very well, but it usually needs very good mesh refinement near contact regions to obtain satisfactory results which makes the time consumption increase considerably. For the FEM with contact elements [12-14], the shortcoming of poor convergence for nonlinear contact analysis has to be overcome. Therefore, the hybrid of FEM and AM [15-17] was more widely used in recent years, which combined the advantages of both of them to get higher computational efficiency than FEM and

stronger structure adaptability than AM.

Compared with the external gears, literatures on the mesh stiffness of internal gears are much fewer. Marques [18] approximated the time-varying mesh stiffness by the principle that the curves of mesh stiffness and the instantaneous length of contact lines are similar to each other. Liang [19] studied the mesh stiffness of spur external and internal gear pairs using the potential energy method, and then Rezaei [20] extended it to helical gears combined with the thin slice theory. Chen [21-24] proposed a model for calculating the mesh stiffness of internal spur gears based on the potential energy principle, and the effects of elastic ring structure, tooth profile shift and tooth rack on the mesh stiffness were analyzed. Karpat [25] investigated the effects of rim thickness and rim shapes on the mesh stiffness of internal gears using 2D finite element models. It was shown from their studies that the gear rim thickness and support parameters affect the internal mesh stiffness a lot. Kahraman [26] studied the effects of ring gear flexibility on the rim stresses under quasi-static conditions by a hybrid of FEM and nonlinear semi-analytical formulae. Recently, Hu and Talbot [27, 28] proposed a comprehensive load distribution model of PGT taking into account the flexible ring gear. Their results showed that the ring flexibility could affect deflections of both gear mesh-level and system-level, and the relative positions of planets and external splines will influence ring deformations, mesh stiffness and load sharing of planets.

In this paper, a method combined of FEM and AM is developed for spur/helical internal gear pairs on the basis of the model by the authors proposed for external gears [16]. The calculation efficiency can be effectively improved compared with conventional FEM, and it could accurately take into account the influence of different ring gear rims as well as the external splines which have not been well considered by a full analytical method.

2. Contact points arrangement in POA

The tooth engagement of an internal gear pair in the transverse section is shown in Fig. 1. N_1 and N_2 are the tangent points of gear base circles with the line of action, and B_1B_2 is the length of path of contact, where B_2 is the start point when the tooth comes into engagement and B_1 is the exit point when the tooth quits engagement. Take B_1B_2 as the height and face with B as the length, the theoretical plane of action (POA) can be obtained, as shown in Fig. 2. The origin o_C of the coordinate system o_C-x_Cy_C locates at point B_2. β_b is the helix angle in the base circle, ε_α and ε_γ are the transverse and total contact ratio of the gear pair, respectively. There are three parallel contact lines in POA at the time shown in Fig. 2. The two adjacent contact lines are one transverse pitch on the base cylinder (p_{bt}) apart in the y_C direction.

The contact points are made uniformly located on the contact lines. The coordinates of point C in POA (x_C, y_C) can be determined in o_C-x_Cy_C by the equations of contact lines in o_C-x_Cy_C and the relative position of point C on its attached contact

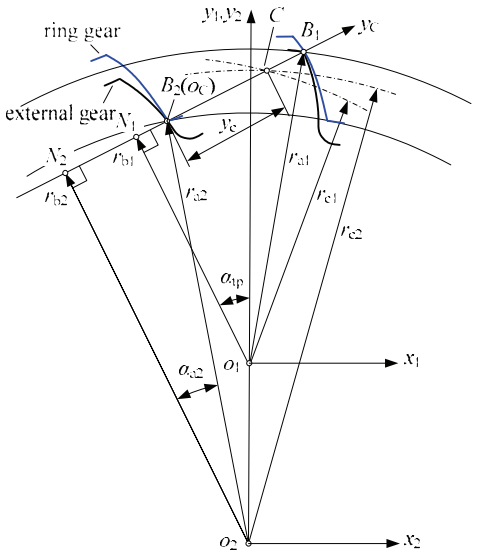

Fig. 1. Schematic representations of the engagement process of an internal gear pair.

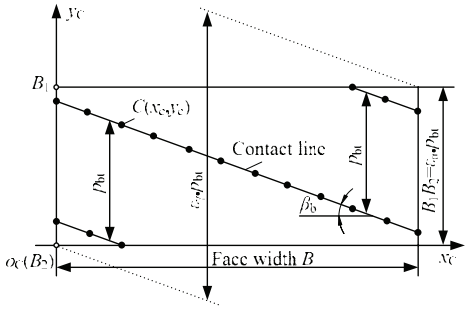

Fig. 2. POA of an internal gear pair when the ring gear is left hand.

line. Then, in accordance with the geometrical relationship in Fig. 1, the radii of the external gear and the ring gear at C can be derived as

$$r_{c1}=\sqrt{(r_{b2}\tan\alpha_{a2}-(r_{b2}-r_{b1})\tan\alpha_{tp}+y_c)^2+r_{b1}^2} \tag{1}$$

$$r_{c2}=\sqrt{(r_{b2}\tan\alpha_{a2}+y_c)^2+r_{b2}^2} \tag{2}$$

where α_{tp} is the working transverse pressure angle, r_{bi} is the radius of base cylinder for gear i, and α_{a2} is the pressure angle at tip circle of the ring gear.

The coordinates of C in the transverse plane (x_{ti}, y_{ti}) (i = 1, 2) can be acquired by solving the combined equations of involute equations at C and Eq. (3):

$$x_{ti}^2+y_{ti}^2=r_{ci}^2\ . \tag{3}$$

By rotating the transverse coordinates of C along the helix, the coordinates of C in its own coordinate system o_i-$x_iy_iz_i$ can be obtained by

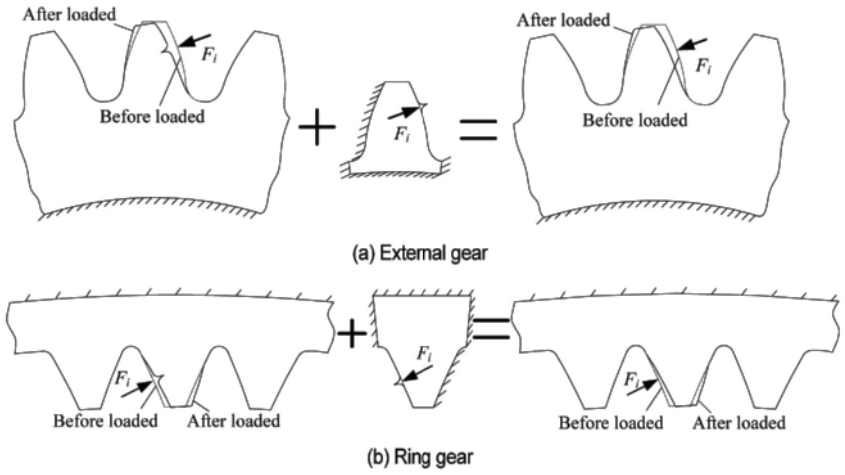

Fig. 3. Separation of linear deformation for external and ring gear.

$$\begin{bmatrix} x_i \\ y_i \\ z_i \end{bmatrix} = \begin{bmatrix} \cos\phi_i & \sin\phi_i & 0 \\ -\sin\phi_i & \cos\phi_i & 0 \\ 0 & 0 & -1 \end{bmatrix} \begin{bmatrix} x_{ti} \\ y_{ti} \\ x_c \end{bmatrix} \tag{4}$$

where $\phi_i = x_c \tan\beta_{bi} / r_{bi}$. β_{bi} is the helix angle of gear *i* at base cylinder, which has a positive value when the gear is right hand and a negative value when the gear is left hand.

3. Tooth contact model under load

3.1 Deformation compatibility condition

The deformations of gear tooth are separated into two parts: The global linear part and the local nonlinear part. The global part mainly includes deformation due to tooth bending and shearing, deformation of gear blank, where the local term is typically the contact deformation at the contact points. The deformation compatibility relationship of all candidate contact points in POA can be expressed

$$-[\lambda_G]_n \{F\}_n - \{u_L\}_n + TE + \{Y\}_n = \{\varepsilon\}_n \tag{5}$$

where *n* is the count of candidate contact points, $[\lambda_G]$ is the flexibility matrix due to linear global deformation, $\{F\}$ is the load distribution vector, $\{u_L\}$ is the local contact deformations of contact points, $\{Y\}$ is the residual gap vector of contact points, $\{\varepsilon\}$ is the gap vector of contact points in the unloaded state, which usually includes the tooth backlash, manufacturing errors on tooth flank, tooth modifications and misalignment due to shaft deflections. Here *TE* is the rigid body approach, namely the transmission error in linear displacement along the tooth normal direction.

Vectors of $\{Y\}$ and $\{F\}$ has the following relationship:

$$\begin{cases} Y_i = 0, \ F_i > 0 & \text{point } i \text{ within contact} \\ Y_i > 0, \ F_i = 0 & \text{point } i \text{ outside contact .} \end{cases} \tag{6}$$

3.2 Separation of linear global deformation using FEM

To obtain accurate local deformations in FEM, the finite element meshes near contact regions must be very refined. For relatively coarse meshes in a FE model, the local deformation near the loading area is inaccurate, while the global bending-shearing deformation far from the loading point is still reliable. Therefore, the global deformation of each contact point could be separated using two FE models, where the separation principle is shown in Fig. 3. A unit normal force is applied to the whole FE model to obtain the total displacement of the loading point, and an opposite unit normal force is applied at the same node in a partial FE model to calculate the local displacement of the loading point. Because only macro deformation is calculated, the FE meshes need not be very dense, which will greatly reduce the calculation consumption.

The flexibility matrix of FE nodes on the concerned tooth flank could be quickly extracted by a substructure analysis. This method can avoid multiple static calculations in conventional ways and reduce the computational effort remarkably [16]. Define the gear FE model as a substructure and the concerned tooth flank as a super element. By condensation of the interior degrees of freedom, the element stiffness matrix of the super element can be calculated. Then the flexibility matrix for the tooth flank could be acquired by inversing the element stiffness matrix. By using the parametric design language of ANSYS software, the FE models can be established automatically and then the substructure analysis can be completed.

The FE nodes of the concerned tooth flank for both the whole and partial FE models are set to distribute uniformly along the tooth profile and the lead direction as well. The node coordinates coincide with each other to accurately remove the local distortion of a certain node from its total deformation. The FE model of the gear is divided into regular hexahedron elements, which can usually obtain better results than the tetrahedron element. By projecting all the contact points and FE modes on the POA, as shown in Fig. 4, the global flexibility

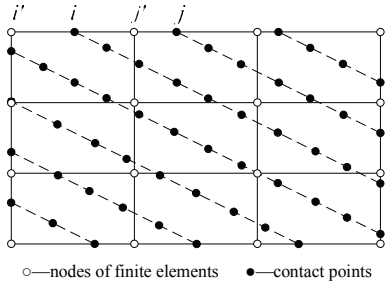

Fig. 4. FE nodes and contact points in POA.

matrix of contact points of tooth flank is obtained by two-dimensional interpolation through the coordinate relationships between them. In order to ensure the accuracy, a biharmonic spline interpolation method [29] is used in this study. It had been proved that this algorithm has higher accuracy than the commonly used cubic interpolation.

3.3 Nonlinear contact deformation by analytical formula

The local deformation of a contact point is substituted by the line contact deformation of the corresponding subsection contact line at that point. The contact deformation u_{Li} can be obtained by the expression [30]

$$u_{Li}=\frac{F_i}{\pi l_i E^*}\ln\frac{6.59 l_i^3 E^*(R_{i2}-R_{i1})}{F_i R_{i1} R_{i2}} \tag{7}$$

where F_i is the contact force at point i, R_{i1} and R_{i2} represent the radius of curvature at point i for two gears, l_i is the subsection contact length which point i occupies, $E^*=1/[(1-v_1^2)/E_1+(1-v_2^2)/E_2]$, and E_1 and E_2 are the Young's modulus, v_1 and v_2 are the Poisson's ratio.

3.4 Solution of contact equations for internal gear pair

The relationships between the contact forces and total mesh force gives the load equilibrium equations:

$$\{I\}_{1\times n}\{F\}_{n\times 1}=P. \tag{8}$$

Eqs. (5) and (8) make up the constrain conditions of the loaded tooth contact model for an internal gear pair, which has n+1 equations. The flexibility matrix $[\lambda_G]$, the initial separations $\{\varepsilon\}$ and the total mesh force P are the known variables in advance, and the load distribution $\{F\}$, the residual separation $\{Y\}$ and transmission error TE are the 2n+1 variables to be determined. By additionally checking the contact statuses of each contact points in Eq. (6), the nonlinear contact equations have unique solution.

The detailed iterative algorithm is given as follows:

Step 1: Assuming that the initial load is uniformly distributed at all theoretical contact points, that is $F_{i(1)}=P/n$, to get the initial load distribution vector $\{F\}_{(1)}$.

Step 2: Calculating the equivalent flexibility matrix for local contact deformation to make the total deformation linear with the contact force.

$$\lambda_{Li}=u_{Li}/F_{i(k)} \qquad i=(1,...n) \tag{9}$$

$$[\lambda_L]_{n(k)}=diag([\lambda_{L1},\lambda_{L2},...,\lambda_{Ln}]). \tag{10}$$

Step 3: By adding the global flexibility matrix $[\lambda_G]$ and local flexibility matrix $[\lambda_L]$ to yield total flexibility $[\lambda]$, nonlinear Eq. (5) can be transformed to linear as Eq. (12).

$$[\lambda]_n=[\lambda_G]_n+[\lambda_L]_n \tag{11}$$

$$-[\lambda]_n\{F\}_n+TE+\{Y\}_n=\{\varepsilon\}_n. \tag{12}$$

Step 4: Now the common contact problem could be solved using a simplex method in Ref. [9] or an iteration method. Here the iteration method is used. It is assumed that all contact points are within contact as the initial condition of inner iteration, which is $\{Y\}=0$. Then Eqs. (8) and (12) can be transformed into linear algebraic equations

$$\begin{cases}-[\lambda]_{na}\{F\}_{na}+TE=\{\varepsilon\}_{na}\\ \{I\}_{na}\{F\}_{na}=P.\end{cases} \tag{13}$$

Because the loads of active contact points are greater than 0, if the solutions of $\{F\}_{na}$ are less than 0, it means that the points do not participate in contact, the rows and columns of the corresponding flexibility matrix $[\lambda]$ and vector $\{\varepsilon\}$ are delimited. The new scale-reduced equations will be solved again until all loads in $\{F\}_{na}$ are greater than 0, and the convergent solution of the inner iteration $\{F\}_{(k+1)}$ and $TE_{(k+1)}$ can be obtained.

Step 5: Judging the difference between two consecutive TEs is less than given tolerance eps or not. If not, $k=k+1$, go **step 2**; else, it means that the load vector has approached the real load distribution, the outer iteration ends.

The iterative flow chart is shown in Fig. 5.

Once $\{F\}$ and TE are obtained, the stiffness of every contact pair k_i can be derived by the deformation relationship in Fig. 6. By adding the stiffness of each contact point within contact, we can get the mesh stiffness of the gear pair as

$$K=\sum_{i=1}^{n}k_i=\sum_{i=1}^{n}\frac{F_i}{\delta_i}=\sum_{i=1}^{n}\frac{F_i}{TE-\varepsilon_i}. \tag{14}$$

4. Model verification and discussion

4.1 Comparisons with FEM and Chen's method

Chen and Shao proposed an analytical method of predicting the mesh stiffness of internal spur gears based on the analytical potential energy method. The flexibility of the ring gear and

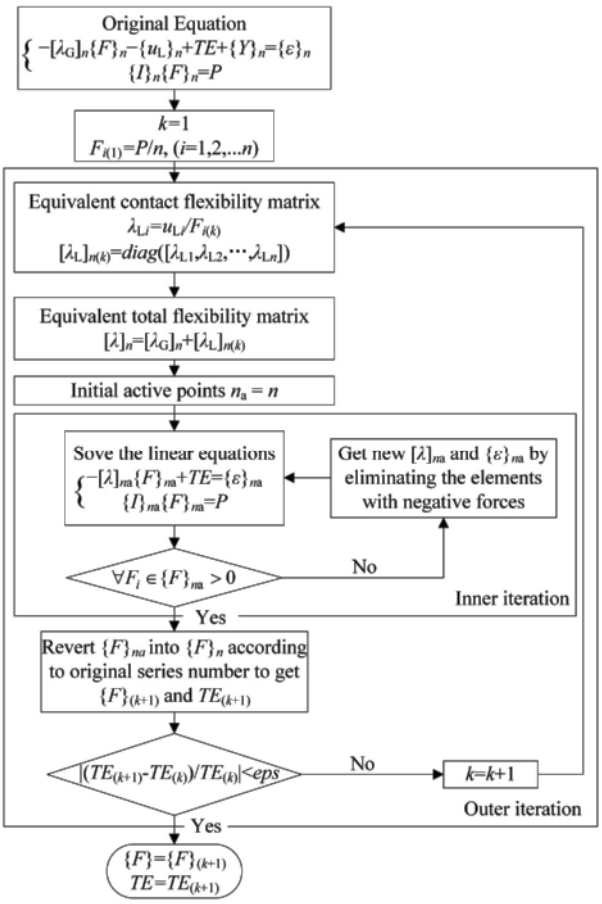

Fig. 5. Algorithm to solve the nonlinear tooth contact equations.

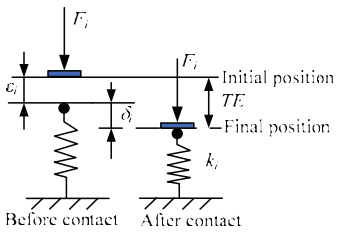

Fig. 6. Relationships when a contact point pair come into contact.

different support types can be considered, and the results were compared with FEM [21, 22]. For comparison, the same parameters of the internal gear pair are used in this paper, as shown in Table 1. The normal mesh force is 300 N/mm according to calculation method in ISO6336. The ring gear has uniformly distributed pins supported on the outer frame, and has a gap between the outer frame, as shown in Fig. 7. Fig. 8 shows the finite element model of the external gear and the ring gear with 4 pins. The middle tooth of three remaining teeth is the one we concerned about. Because the FE model is only used to calculate the global deformation, so the elements of the teeth surfaces and the teeth roots need not be very dense. The circumferential DOFs of FE nodes at the arcs where the pins connected with the ring gear are constrained, and these nodes

Table 1. Parameters of the internal gear pair in Ref. [21].

Parameter	Value
Number of teeth of external gear N_1	20
Number of teeth of ring gear N_2	70
Normal module m_n/mm	1.7
Normal pressure angle α_n/(°)	21.34
Helix angle β/(°)	0
Face width B/mm	25
Young's modulus E/GPa	205
Poisson's ratio ν	0.3
Normal mesh force P/N	7500

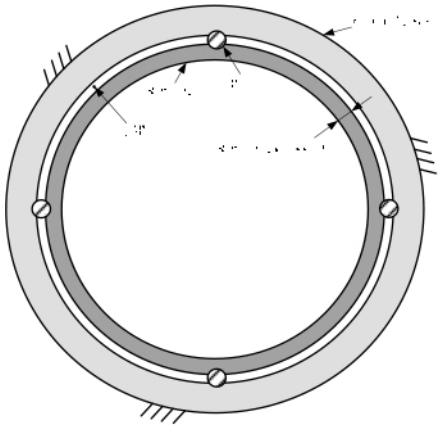

Fig. 7. Structure of the ring gear with pin support.

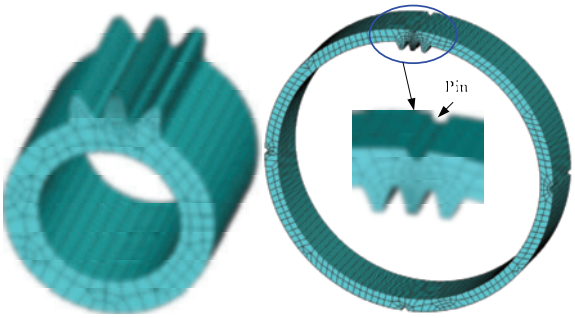

(a) External gear (b) Ring gear

Fig. 8. Finite element model of the external gear and the ring gear.

can only move along the radial direction to simulate the supports of pins.

Chen calculated the single stiffness in the case of the mesh force acting on the tip of ring gear teeth, and verified it by a finite element method. The stiffnesses calculated by the proposed method, FEM and Chen's method with different number of support pins Ns are shown in Fig. 9. The ring thickness keeps as 6 mm. Because the pins are uniformly distributed, only the mesh stiffness between pin 1 and pin 2 are given. It can be observed from this figure that the three stiffness curves

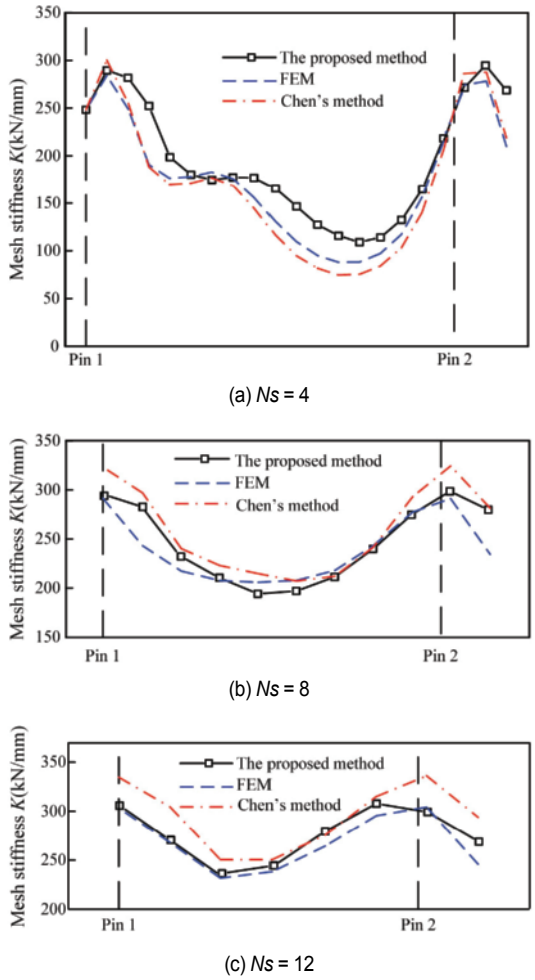

Fig. 9. Single mesh stiffness at the addendum of ring gear tooth.

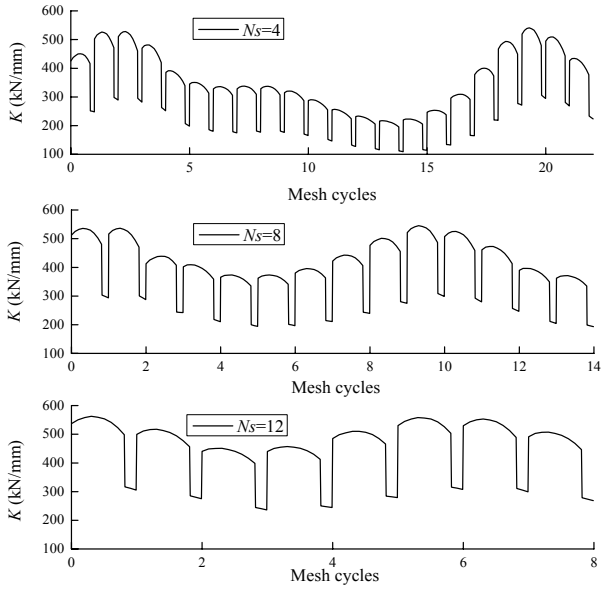

Fig. 10. Mesh stiffness when ring gear has different number of support pins.

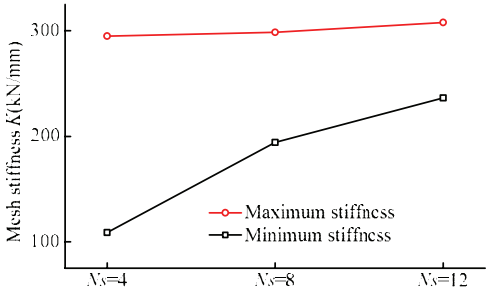

Fig. 11. Maximum and minimum mesh stiffness with different number of support pins.

are close to each other, which proves the effectiveness of the proposed method. Because the results calculated by FEM are obviously influenced by the mesh density, and the detailed parameters, such as the angular position between the ring gear tooth and its neighboring pins, the pin size, were not given in Ref. [21], there are slight differences between the FEM results and the proposed method.

As to the computational efficiency, Chen's analytical method required minimum time consumption, but it can be only used for spur gears and smooth external gear/ring body. For helical gears, or the irregular structured gears, the analytical method will lose effectiveness. The specific process of FE analysis in Ref. [21] was not described in detail. However, both conventional FEM and FEM with contact elements need high mesh density. Especially for the contact FEM involving large-scale nonlinear iterative calculation, the calculation usually takes several hours and the convergence is also rather poor. For the proposed method in this paper, a much lower mesh density of FE model is required due to only the global deformation is calculated in one static analysis, which will significantly reduce the calculation time. For the examples here, the time consumption of the proposed method is about 2 min in a personal computer.

4.2 Effects of number of support pins

The mesh stiffness with different number of support pins *Ns* are illustrated in Fig. 10. Similar to the single mesh stiffness, the total mesh stiffness changes periodically along the circumference of the ring gear. In the figure, the stiffness curve is composed of two frequency components. The high frequency is caused by the alternation contact of single and double teeth, while the low frequency is caused by the flexibility of ring gear and is related to *Ns*. The amplitude of total mesh stiffness is larger near the support pin position and smaller away from the support pin position. Since the number of teeth is not completely divided by the number of support pins, the mesh stiffness curve varies unevenly in a quasi-periodic manner.

The maximum and minimum mesh stiffness of Fig. 10 are illustrated in Fig. 11 for different *Ns*. The maximum stiffness occurs near the pins, where the tooth deformation is the main part of the total deformation when the ring body deformation is rather small due to the constrains of pins. It is also observed that the maximum stiffness has little change with different *Ns*. The minimum stiffness usually occurs the middle of two pins,

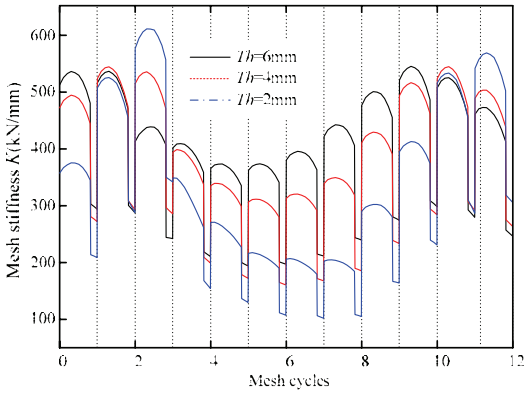

Fig. 12. Mesh stiffness for different ring thicknesses when *Ns* is 8.

where the ring body deformation becomes greater and results in greater total deformation. Moreover, it can be seen from Fig. 11 that greater ring deformation will be produced for less number of support pins, which leads to decreased stiffness than the case with more support pins. That means the peak-to-peak value of the mesh stiffness is reduced when the ring gear has more supports.

4.3 Effects of ring thickness

Fig. 12 shows the mesh stiffness curves with different ring thickness *Th* when the pin number *Ns* is 8. It can be seen that in the area far away from the support pins, the deformation of the thin ring is larger than that of the thick ring, so the mesh stiffness will be decreased as shown in the mesh cycle 4 to 10. But in the area near the support pins, the mesh stiffness of thin ring is almost the same with the thick ones (cycle 2 and 11), and it is even greater than the thick ring (cycle 3 and 12). This is due to the fact that the deformations of the ring differ slightly for different ring thicknesses near the support position, but the bending deformations of thin rings is larger than thick rings because the mesh load on the tooth surface of the thin ring gear is closer to the constraint position than the thick ones. Therefore, the mesh stiffness with *Th* = 2 mm is the largest in this position (cycle 3 and 12).

In addition, it can be found from the figure that the stiffness curves of each mesh cycle are different due to the influence of ring flexibility, especially in the area with double teeth contact. The high- and low-frequency components of mesh stiffness will both change a lot for different ring thicknesses. If subsequent dynamic analysis is needed, this effect must be taken in account to obtain more accurate prediction results.

5. Conclusions

This paper presents a method for determining the mesh stiffness of spur/helical internal gear pairs combining the FEM and analytical contact theory. This method can accurately take into account the influence of flexible ring gear with different ring structures as conventional FEM does, but has higher efficiency than conventional FEM. Effects of the ring structures on the mesh stiffness is studied. It can be found from the results the mesh stiffness near the middle of the support pins is smaller than that near the support pins. With the increase of the number of pins, the mesh stiffness at the middle position of the support pins is getting increased. The mesh stiffness for a ring gear with a larger thickness is greater than that with a smaller thickness far from the support position, while it is opposite near the support position. The ring flexibility will affect the amplitude-frequency components of the mesh stiffness of the internal gear pair, which should be considered in subsequent vibration analysis.

Acknowledgments

This paper is supported by the Natural Science Basic Research Program of Shaanxi (Grant No. 2019JQ-695, 2018JQ5059), National Natural Science Foundation of China (Grant No. 51605040), and the China Postdoctoral Science Foundation (Grant No. 2018M640943).

Nomenclature

AM : Analytical method
B : Face width
B_1B_2 : Length of path of contact
E_j : Young's modulus of gear j
FE : Finite element
FEM : Finite element method
$\{F\}$: Contact force vector
K : Mesh stiffness of the gear pair
l_i : The subsection contact length of point i
m_n : Normal module
n : Number of total candidate contact points
na : Number of active contact points
N_j : Number of teeth of gear j
Ns : Number of support pins
p_{bt} : Transverse pitch on the base cylinder
P : Total mesh force
POA : Plane of action
r_{bi} : Radius of base circle for gear i
r_{ci} : Radius of contact point C
R_{ij} : Radius of curvature at point i for gear j
TE : Transmission error along LOA
Th : Ring thickness
u_{Li} : Contact deformation of contact point i
$\{u_L\}$: Vector of local contact deformations
x_i,y_i,z_i : Coordinates of contact point C in coordinate system o_i-$x_iy_iz_i$
x_C, y_C : Coordinates of contact point C in coordinate system o_C-x_Cy_C
x_{ti}, y_{ti} : Coordinates of contact point C in transverse plane
$\{Y\}$: Residual gap vector after contact
α_{ai} : Transverse pressure angle at tip circle of gear i
α_{tp} : Working transverse pressure angle

α_n : Normal pressure angle
β : Helix angle
β_b : Base helix angle
ε_α : Transverse contact ratio
ε_γ : Total contact ratio
$\{\varepsilon\}$: Unloaded separation distance vector
$[\lambda_G]$: Global flexibility matrix
$[\lambda_L]$: Equivalent contact flexibility matrix
$[\lambda]$: Equivalent total flexibility matrix
v_j : Poisson's ratio of gear j

References

[1] C. Weber, *The Deformations of Loaded Gears and the Effect on Their Load-carrying Capacity*, British Dept. of Scientific and Industrial Research, Report No. 3 (1949).

[2] J. Ishikawa, On the deflection of gear teeth, *Bulletin of the JSME*, 17 (59) (1951) 103-106.

[3] Y. Terauchi and K. Nagamura, Study on deflection of spur gear teeth (1st Report), *Bulletin of JSME*, 23 (1980) 1682-1688.

[4] P. Sainsot, P. Velex and O. Duverger, Contribution of gear body to tooth deflections - A new bidimensional analytical formula, *Journal of Mechanical Design*, *Transactions of the ASME*, 126 (7) (2004) 748-752.

[5] J. Börner, M. Maier and F. J. Joachim, Design of transmission gearings for low noise emission-loaded tooth contact analysis with automated parameter variation, *International Conference on Gears 2013* (2013) 719-730.

[6] Z. G. Wan et al., Mesh stiffness calculation using an accumulated integral potential energy method and dynamic analysis of helical gears, *Mechanism and Machine Theory*, 92 (2015) 447-463.

[7] Q. B. Wang and Y. M. Zhang, A model for analyzing stiffness and stress in a helical gear pair with tooth profile errors, *Journal of Vibration & Control*, 23 (2) (2015) 272-289.

[8] M. J. Feng et al., An improved analytical method for calculating time-varying mesh stiffness of helical gears, *Meccanica*, 53 (2018) 1131-1145.

[9] S. T. Li, Gear contact model and loaded tooth contact analysis of a three-dimensional thin-rimmed gear, *Journal of Mechanical Design*, 124 (2002) 511-517.

[10] S. T. Li, Effects of machining errors, assembly errors and tooth modifications on loading capacity, load-sharing ratio and transmission error of a pair of spur gears, *Mechanism and Machine Theory*, 42 (2007) 698-726.

[11] S. Y. Ye and S. J. Tsai, A computerized method for loaded tooth contact analysis of high-contact-ratio spur gears with or without flank modification considering tip corner contact and shaft misalignment, *Mechanism and Machine Theory*, 97 (2016) 190-214.

[12] T. J. Lin, H. Ou and R. F. Li, A finite element method for 3D static and dynamic contact/impact analysis of gear drives, *Computer Methods in Applied Mechanics and Engineering*, 196 (2007) 1716-1728.

[13] T. Kiekbusch et al., Calculation of the combined torsional mesh stiffness of spur gear with two- and three-dimensional parametrical FE models, *Journal of Mechanical Engineering*, 57 (2007) 810-818.

[14] S. Y. Liu et al., Investigation on the influence of work holding equipment errors on contact characteristics of face-hobbed hypoid gear, *Mechanism and Machine Theory*, 138 (2019) 95-111.

[15] A. Fernández et al., A model for the study of meshing stiffness in spur gear transmissions, *Mechanism and Machine Theory*, 61 (2013) 30-58.

[16] L. H. Chang, G. Liu and L. Y. Wu, A robust model for determining the mesh stiffness of cylindrical gears, *Mechanism and Machine Theory*, 87 (2015) 93-114.

[17] Q. B. Wang et al., An analytical-finite-element method for calculating mesh stiffness of spur gear pairs with complicated foundation and crack, *Engineering Failure Analysis*, 94 (2018) 339-353.

[18] P. Marques, R. Martins and J. Seabra, Analytical load sharing and mesh stiffness model for spur/helical and internal/external gears – towards constant mesh stiffness gear design, *Mechanism and Machine Theory*, 113 (2017) 126-140.

[19] X. H. Liang, M. J. Zuo and T. H. Patel, Evaluating the time-varying mesh stiffness of a planetary gear set using the potential energy method, *Proceedings of the Institution of Mechanical Engineers, Part C: Journal of Mechanical Engineering Science*, 228 (3) (2014) 535-547.

[20] M. Rezaei et al., Calculation of time dependent mesh stiffness of helical planetary gear system using analytical approach, *Journal of Mechanical Science and Technology*, 32 (8) (2018) 3537-3545.

[21] Z. G. Chen and Y. M. Shao, Mesh stiffness of an internal spur gear pair with ring gear rim deformation, *Mechanism and Machine Theory*, 69 (2013) 1-12.

[22] Z. G. Chen, Study on gear mesh nonlinear excitation modelling and vibration features of planetary gear system, *Ph.D. Dissertation*, Chongqing University (2013).

[23] Z. G. Chen, Z. F. Zhu and Y. M. Shao, Fault feature analysis of planetary gear system with tooth root crack and flexible ring gear rim, *Engineering Failure Analysis*, 49 (2015) 92-103.

[24] Z. G. Chen et al., Mesh stiffness evaluation of an internal spur gear pair with tooth profile shift, *Science China Technological Sciences*, 59 (2016) 1328-1339.

[25] F. Karpat et al., Effects of rim thickness on tooth root stress and mesh stiffness of internal gears, *Proceedings of the ASME 2014 International Mechanical Engineering Congress and Exposition*, Canada (2014).

[26] A. Kahraman and S. Vijayakar, Effect of internal gear flexibility on the quasi-static behavior of a planetary gear set, *Journal of Mechanical Design*, 123 (2001) 408-415.

[27] Y. Hu, D. Talbot and A. Kahraman, A load distribution model for planetary gear sets, *Journal of Mechanical Design*, 140 (2018) 053302.

[28] Y. Hu, D. Talbot and A. Kahraman, A gear load distribution model for a planetary gear set with a flexible ring gear having external splines, *Journal of Mechanical Design*, 141 (2019)

053301.
[29] D. T. Sandwell, Biharmonic spline interpolation of GEOS-3 and seasat altimeter data, *Geophysical Research Letters,* 14 (1987) 139-142.
[30] C. A. Ding, L. Zhang and F. Z. Zhou, Theoretical formula for calculation of line-contact elastic contact deformation, *Tribology*, 21 (2001) 135-138.

Shuo Feng is a Lecturer at School of Construction Machinery, Chang'an University, Xi'an, China. He received his Ph.D. degree in Northwestern Polytechnical University (NWPU), China. His research interests include mechanical strength and reliability, mechanical system dynamics, robotics, artificial intelligence and others.

Lehao Chang is an Associate Professor at School of Construction Machinery, Chang'an University, Xi'an, China. He received his Ph.D. degree in Northwestern Polytechnical University (NWPU), China. His research interests include gear contact theory, geared rotor system dynamics, and others. He has published more than 20 journal and conference papers.

Zhaoxia He is an Associate Professor at Chang'an University, Xi'an, China, and now serves as Assistant Dean of the School of Construction Machinery. She received her Ph.D. degree in Northwestern Polytechnical University (NWPU), China. Her research interests include mechanical system dynamics, gear system dynamics modeling and simulation, virtual prototype technology, and so on. She has published more than 30 journal and conference papers.